PHYSICAL REVIEW D **72,** 011104(R) (2005)

Search for right-handed *W* bosons in top quark decay

V. M. Abazov,[35] B. Abbott,[72] M. Abolins,[63] B. S. Acharya,[29] M. Adams,[50] T. Adams,[48] M. Agelou,[18] J.-L. Agram,[19] S. H. Ahn,[31] M. Ahsan,[57] G. D. Alexeev,[35] G. Alkhazov,[39] A. Alton,[62] G. Alverson,[61] G. A. Alves,[2] M. Anastasoaie,[34] T. Andeen,[52] S. Anderson,[44] B. Andrieu,[17] Y. Arnoud,[14] A. Askew,[48] B. Åsman,[40] A. C. S. Assis Jesus,[3] O. Atramentov,[55] C. Autermann,[21] C. Avila,[8] F. Badaud,[13] A. Baden,[59] B. Baldin,[49] P. W. Balm,[33] S. Banerjee,[29] E. Barberis,[61] P. Bargassa,[76] P. Baringer,[56] C. Barnes,[42] J. Barreto,[2] J. F. Bartlett,[49] U. Bassler,[17] D. Bauer,[53] A. Bean,[56] S. Beauceron,[17] M. Begel,[68] A. Bellavance,[65] S. B. Beri,[27] G. Bernardi,[17] R. Bernhard,[49,*] I. Bertram,[41] M. Besançon,[18] R. Beuselinck,[42] V. A. Bezzubov,[38] P. C. Bhat,[49] V. Bhatnagar,[27] M. Binder,[25] C. Biscarat,[41] K. M. Black,[60] I. Blackler,[42] G. Blazey,[51] F. Blekman,[42] S. Blessing,[48] D. Bloch,[19] U. Blumenschein,[23] A. Boehnlein,[49] O. Boeriu,[54] T. A. Bolton,[57] F. Borcherding,[49] G. Borissov,[41] K. Bos,[33] T. Bose,[67] A. Brandt,[74] R. Brock,[63] G. Brooijmans,[67] A. Bross,[49] N. J. Buchanan,[48] D. Buchholz,[52] M. Buehler,[50] V. Buescher,[23] S. Burdin,[49] T. H. Burnett,[78] E. Busato,[17] C. P. Buszello,[42] J. M. Butler,[60] J. Cammin,[68] S. Caron,[33] W. Carvalho,[3] B. C. K. Casey,[73] N. M. Cason,[54] H. Castilla-Valdez,[32] S. Chakrabarti,[29] D. Chakraborty,[51] K. M. Chan,[68] A. Chandra,[29] D. Chapin,[73] F. Charles,[19] E. Cheu,[44] D. K. Cho,[60] S. Choi,[47] B. Choudhary,[23] T. Christiansen,[25] L. Christofek,[56] D. Claes,[65] B. Clément,[19] C. Clément,[40] Y. Coadou,[5] M. Cooke,[76] W. E. Cooper,[49] D. Coppage,[56] M. Corcoran,[76] A. Cothenet,[15] M.-C. Cousinou,[15] B. Cox,[43] S. Crépé-Renaudin,[14] D. Cutts,[73] H. da Motta,[2] M. Das,[58] B. Davies,[41] G. Davies,[42] G. A. Davis,[52] K. De,[74] P. de Jong,[33] S. J. de Jong,[34] E. De La Cruz-Burelo,[32] C. De Oliveira Martins,[3] S. Dean,[43] J. D. Degenhardt,[62] F. Déliot,[18] M. Demarteau,[49] R. Demina,[68] P. Demine,[18] D. Denisov,[49] S. P. Denisov,[38] S. Desai,[69] H. T. Diehl,[49] M. Diesburg,[49] M. Doidge,[41] H. Dong,[69] S. Doulas,[61] L. V. Dudko,[37] L. Duflot,[16] S. R. Dugad,[29] A. Duperrin,[15] J. Dyer,[63] A. Dyshkant,[51] M. Eads,[51] D. Edmunds,[63] T. Edwards,[43] J. Ellison,[47] J. Elmsheuser,[25] V. D. Elvira,[49] S. Eno,[59] P. Ermolov,[37] O. V. Eroshin,[38] J. Estrada,[49] H. Evans,[67] A. Evdokimov,[36] V. N. Evdokimov,[38] J. Fast,[49] S. N. Fatakia,[60] L. Feligioni,[60] A. V. Ferapontov,[38] T. Ferbel,[68] F. Fiedler,[25] F. Filthaut,[34] W. Fisher,[66] H. E. Fisk,[49] I. Fleck,[23] M. Fortner,[51] H. Fox,[23] S. Fu,[49] S. Fuess,[49] T. Gadfort,[78] C. F. Galea,[34] E. Gallas,[49] E. Galyaev,[54] C. Garcia,[68] A. Garcia-Bellido,[78] J. Gardner,[56] V. Gavrilov,[36] A. Gay,[19] P. Gay,[13] D. Gelé,[19] R. Gelhaus,[47] K. Genser,[49] C. E. Gerber,[50] Y. Gershtein,[48] D. Gillberg,[5] G. Ginther,[68] B. Gmyrek,[44] T. Golling,[22] N. Gollub,[40] B. Gómez,[8] K. Gounder,[49] A. Goussiou,[54] P. D. Grannis,[69] S. Greder,[3] H. Greenlee,[49] Z. D. Greenwood,[58] E. M. Gregores,[4] Ph. Gris,[13] J.-F. Grivaz,[16] L. Groer,[67] S. Grünendahl,[49] M. W. Grünewald,[30] S. N. Gurzhiev,[38] G. Gutierrez,[49] P. Gutierrez,[72] A. Haas,[67] N. J. Hadley,[59] S. Hagopian,[48] I. Hall,[72] R. E. Hall,[46] C. Han,[62] L. Han,[7] K. Hanagaki,[49] K. Harder,[57] A. Harel,[26] R. Harrington,[61] J. M. Hauptman,[55] R. Hauser,[63] J. Hays,[52] T. Hebbeker,[21] D. Hedin,[51] J. M. Heinmiller,[50] A. P. Heinson,[57] U. Heintz,[60] C. Hensel,[56] G. Hesketh,[61] M. D. Hildreth,[54] R. Hirosky,[77] J. D. Hobbs,[69] B. Hoeneisen,[12] M. Hohlfeld,[24] S. J. Hong,[31] R. Hooper,[73] P. Houben,[33] Y. Hu,[69] J. Huang,[53] V. Hynek,[9] I. Iashvili,[47] R. Illingworth,[49] A. S. Ito,[49] S. Jabeen,[56] M. Jaffré,[16] S. Jain,[72] V. Jain,[70] K. Jakobs,[23] A. Jenkins,[42] R. Jesik,[42] K. Johns,[44] M. Johnson,[49] A. Jonckheere,[49] P. Jonsson,[42] A. Juste,[49] D. Käfer,[21] S. Kahn,[70] E. Kajfasz,[15] A. M. Kalinin,[35] J. Kalk,[63] D. Karmanov,[37] J. Kasper,[60] D. Kau,[48] R. Kaur,[27] R. Kehoe,[75] S. Kermiche,[15] S. Kesisoglou,[73] A. Khanov,[68] A. Kharchilava,[54] Y. M. Kharzheev,[35] H. Kim,[74] T. J. Kim,[31] B. Klima,[49] J. M. Kohli,[27] M. Kopal,[72] V. M. Korablev,[38] J. Kotcher,[70] B. Kothari,[67] A. Koubarovsky,[37] A. V. Kozelov,[38] J. Kozminski,[63] A. Kryemadhi,[77] S. Krzywdzinski,[49] Y. Kulik,[49] A. Kumar,[28] S. Kunori,[59] A. Kupco,[11] T. Kurča,[20] J. Kvita,[9] S. Lager,[40] N. Lahrichi,[18] G. Landsberg,[73] J. Lazoflores,[48] A.-C. Le Bihan,[19] P. Lebrun,[20] W. M. Lee,[48] A. Leflat,[37] F. Lehner,[49,*] C. Leonidopoulos,[67] J. Leveque,[44] P. Lewis,[42] J. Li,[74] Q. Z. Li,[49] J. G. R. Lima,[51] D. Lincoln,[49] S. L. Linn,[48] J. Linnemann,[63] V. V. Lipaev,[38] R. Lipton,[49] L. Lobo,[42] A. Lobodenko,[39] M. Lokajicek,[11] A. Lounis,[19] P. Love,[41] H. J. Lubatti,[78] L. Lueking,[49] M. Lynker,[54] A. L. Lyon,[49] A. K. A. Maciel,[51] R. J. Madaras,[45] P. Mättig,[26] C. Magass,[21] A. Magerkurth,[62] A.-M. Magnan,[14] N. Makovec,[16] P. K. Mal,[29] H. B. Malbouisson,[3] S. Malik,[65] V. L. Malyshev,[35] H. S. Mao,[6] Y. Maravin,[49] M. Martens,[49] S. E. K. Mattingly,[73] A. A. Mayorov,[38] R. McCarthy,[69] R. McCroskey,[44] D. Meder,[24] A. Melnitchouk,[64] A. Mendes,[15] M. Merkin,[37] K. W. Merritt,[49] A. Meyer,[21] J. Meyer,[22] M. Michaut,[18] H. Miettinen,[76] J. Mitrevski,[67] J. Molina,[3] N. K. Mondal,[29] R. W. Moore,[5] T. Moulik,[56] G. S. Muanza,[20] M. Mulders,[49] Y. D. Mutaf,[69] E. Nagy,[15] M. Narain,[60] N. A. Naumann,[34] H. A. Neal,[62] J. P. Negret,[8] S. Nelson,[48] P. Neustroev,[39] C. Noeding,[23] A. Nomerotski,[49] S. F. Novaes,[4] T. Nunnemann,[25] E. Nurse,[43] V. O'Dell,[49] D. C. O'Neil,[5] V. Oguri,[3] N. Oliveira,[3] N. Oshima,[49] G. J. Otero y Garzón,[50] P. Padley,[76] N. Parashar,[58] S. K. Park,[31] J. Parsons,[67] R. Partridge,[73] N. Parua,[69] A. Patwa,[70] G. Pawloski,[76] P. M. Perea,[47] E. Perez,[18] P. Pétroff,[16] M. Petteni,[42] R. Piegaia,[1] M.-A. Pleier,[68] P. L. M. Podesta-Lerma,[32] V. M. Podstavkov,[49] Y. Pogorelov,[54] A. Pompoš,[72] B. G. Pope,[63] W. L. Prado da Silva,[3] H. B. Prosper,[48] S. Protopopescu,[70] J. Qian,[62] A. Quadt,[22] B. Quinn,[64] K. J. Rani,[29] K. Ranjan,[28]

P. A. Rapidis,[49] P. N. Ratoff,[41] S. Reucroft,[61] M. Rijssenbeek,[69] I. Ripp-Baudot,[19] F. Rizatdinova,[57] S. Robinson,[42] R. F. Rodrigues,[3] C. Royon,[19] P. Rubinov,[49] R. Ruchti,[54] V. I. Rud,[37] G. Sajot,[14] A. Sánchez-Hernández,[32] M. P. Sanders,[54] A. Santoro,[3] G. Savage,[49] L. Sawyer,[58] T. Scanlon,[42] D. Schaile,[25] R. D. Schamberger,[69] H. Schellman,[52] P. Schieferdecker,[25] C. Schmitt,[26] C. Schwanenberger,[22] A. Schwartzman,[66] R. Schwienhorst,[63] S. Sengupta,[48] H. Severini,[72] E. Shabalina,[50] M. Shamim,[57] V. Shary,[18] A. A. Shchukin,[38] W. D. Shephard,[54] R. K. Shivpuri,[28] D. Shpakov,[61] R. A. Sidwell,[57] V. Simak,[10] V. Sirotenko,[49] P. Skubic,[72] P. Slattery,[68] R. P. Smith,[49] K. Smolek,[10] G. R. Snow,[65] J. Snow,[71] S. Snyder,[70] S. Söldner-Rembold,[43] X. Song,[51] L. Sonnenschein,[17] A. Sopczak,[41] M. Sosebee,[74] K. Soustruznik,[9] M. Souza,[2] B. Spurlock,[74] N. R. Stanton,[57] J. Stark,[14] J. Steele,[58] K. Stevenson,[53] V. Stolin,[36] A. Stone,[50] D. A. Stoyanova,[38] J. Strandberg,[40] M. A. Strang,[74] M. Strauss,[72] R. Ströhmer,[25] D. Strom,[52] M. Strovink,[45] L. Stutte,[49] S. Sumowidagdo,[48] A. Sznajder,[3] M. Talby,[57] P. Tamburello,[44] W. Taylor,[5] P. Telford,[43] J. Temple,[44] M. Tomoto,[49] T. Toole,[59] J. Torborg,[54] S. Towers,[69] T. Trefzger,[24] S. Trincaz-Duvoid,[17] B. Tuchming,[18] C. Tully,[66] A. S. Turcot,[43] P. M. Tuts,[67] L. Uvarov,[39] S. Uvarov,[39] S. Uzunyan,[51] B. Vachon,[5] R. Van Kooten,[53] W. M. van Leeuwen,[33] N. Varelas,[50] E. W. Varnes,[44] A. Vartapetian,[74] I. A. Vasilyev,[38] M. Vaupel,[26] P. Verdier,[20] L. S. Vertogradov,[35] M. Verzocchi,[59] F. Villeneuve-Seguier,[42] J.-R. Vlimant,[17] E. Von Toerne,[57] M. Vreeswijk,[33] T. Vu Anh,[16] H. D. Wahl,[48] L. Wang,[59] J. Warchol,[54] G. Watts,[78] M. Wayne,[54] M. Weber,[49] H. Weerts,[63] N. Wermes,[22] A. White,[74] V. White,[49] D. Wicke,[49] D. A. Wijngaarden,[34] G. W. Wilson,[56] S. J. Wimpenny,[47] J. Wittlin,[60] M. Wobisch,[49] J. Womersley,[49] D. R. Wood,[61] T. R. Wyatt,[43] Q. Xu,[62] N. Xuan,[54] S. Yacoob,[52] R. Yamada,[49] M. Yan,[59] T. Yasuda,[49] Y. A. Yatsunenko,[35] Y. Yen,[26] K. Yip,[70] H. D. Yoo,[73] S. W. Youn,[52] J. Yu,[74] A. Yurkewicz,[69] A. Zabi,[16] A. Zatserklyaniy,[51] M. Zdrazil,[69] C. Zeitnitz,[24] D. Zhang,[49] X. Zhang,[72] T. Zhao,[78] Z. Zhao,[62] B. Zhou,[62] J. Zhu,[69] M. Zielinski,[68] D. Zieminska,[53] A. Zieminski,[53] R. Zitoun,[69] V. Zutshi,[51] and E. G. Zverev[37]

(D0 Collaboration)

[1]*Universidad de Buenos Aires, Buenos Aires, Argentina*
[2]*LAFEX, Centro Brasileiro de Pesquisas Físicas, Rio de Janeiro, Brazil*
[3]*Universidade do Estado do Rio de Janeiro, Rio de Janeiro, Brazil*
[4]*Instituto de Física Teórica, Universidade Estadual Paulista, São Paulo, Brazil*
[5]*University of Alberta, Edmonton, Alberta, Canada, Simon Fraser University, Burnaby, British Columbia, Canada, York University, Toronto, Ontario, Canada, and McGill University, Montreal, Quebec, Canada*
[6]*Institute of High Energy Physics, Beijing, People's Republic of China*
[7]*University of Science and Technology of China, Hefei, People's Republic of China*
[8]*Universidad de los Andes, Bogotá, Colombia*
[9]*Center for Particle Physics, Charles University, Prague, Czech Republic*
[10]*Czech Technical University, Prague, Czech Republic*
[11]*Center for Particle Physics, Institute of Physics, Academy of Sciences of the Czech Republic, Prague, Czech Republic*
[12]*Universidad San Francisco de Quito, Quito, Ecuador*
[13]*Laboratoire de Physique Corpusculaire, IN2P3-CNRS, Université Blaise Pascal, Clermont-Ferrand, France*
[14]*Laboratoire de Physique Subatomique et de Cosmologie, IN2P3-CNRS, Universite de Grenoble 1, Grenoble, France*
[15]*CPPM, IN2P3-CNRS, Université de la Méditerranée, Marseille, France*
[16]*IN2P3-CNRS, Laboratoire de l'Accélérateur Linéaire, Orsay, France*
[17]*LPNHE, IN2P3-CNRS, Universités Paris VI and VII, Paris, France*
[18]*DAPNIA/Service de Physique des Particules, CEA, Saclay, France*
[19]*IReS, IN2P3-CNRS, Université Louis Pasteur, Strasbourg, France, and Université de Haute Alsace, Mulhouse, France*
[20]*Institut de Physique Nucléaire de Lyon, IN2P3-CNRS, Université Claude Bernard, Villeurbanne, France*
[21]*Physikalisches Institut A, RWTH Aachen, Aachen, Germany*
[22]*Physikalisches Institut, Universität Bonn, Bonn, Germany*
[23]*Physikalisches Institut, Universität Freiburg, Freiburg, Germany*
[24]*Institut für Physik, Universität Mainz, Mainz, Germany*
[25]*Ludwig-Maximilians-Universität München, München, Germany*
[26]*Fachbereich Physik, University of Wuppertal, Wuppertal, Germany*
[27]*Panjab University, Chandigarh, India*
[28]*Delhi University, Delhi, India*
[29]*Tata Institute of Fundamental Research, Mumbai, India*
[30]*University College Dublin, Dublin, Ireland*
[31]*Korea Detector Laboratory, Korea University, Seoul, Korea*
[32]*CINVESTAV, Mexico City, Mexico*

[33]*FOM-Institute NIKHEF and University of Amsterdam/NIKHEF, Amsterdam, The Netherlands*
[34]*Radboud University Nijmegen/NIKHEF, Nijmegen, The Netherlands*
[35]*Joint Institute for Nuclear Research, Dubna, Russia*
[36]*Institute for Theoretical and Experimental Physics, Moscow, Russia*
[37]*Moscow State University, Moscow, Russia*
[38]*Institute for High Energy Physics, Protvino, Russia*
[39]*Petersburg Nuclear Physics Institute, St. Petersburg, Russia*
[40]*Lund University, Lund, Sweden, Royal Institute of Technology, and Stockholm University, Stockholm, Sweden, and Uppsala University, Uppsala, Sweden*
[41]*Lancaster University, Lancaster, United Kingdom*
[42]*Imperial College, London, United Kingdom*
[43]*University of Manchester, Manchester, United Kingdom*
[44]*University of Arizona, Tucson, Arizona 85721, U.S.A.*
[45]*Lawrence Berkeley National Laboratory and University of California, Berkeley, California 94720, U.S.A.*
[46]*California State University, Fresno, California 93740, U.S.A.*
[47]*University of California, Riverside, California 92521, U.S.A.*
[48]*Florida State University, Tallahassee, Florida 32306, U.S.A.*
[49]*Fermi National Accelerator Laboratory, Batavia, Illinois 60510, U.S.A.*
[50]*University of Illinois at Chicago, Chicago, Illinois 60607, U.S.A.*
[51]*Northern Illinois University, DeKalb, Illinois 60115, U.S.A.*
[52]*Northwestern University, Evanston, Illinois 60208, U.S.A.*
[53]*Indiana University, Bloomington, Indiana 47405, U.S.A.*
[54]*University of Notre Dame, Notre Dame, Indiana 46556, U.S.A.*
[55]*Iowa State University, Ames, Iowa 50011, U.S.A.*
[56]*University of Kansas, Lawrence, Kansas 66045, U.S.A.*
[57]*Kansas State University, Manhattan, Kansas 66506, U.S.A.*
[58]*Louisiana Tech University, Ruston, Louisiana 71272, U.S.A.*
[59]*University of Maryland, College Park, Maryland 20742, U.S.A.*
[60]*Boston University, Boston, Massachusetts 02215, U.S.A.*
[61]*Northeastern University, Boston, Massachusetts 02115, U.S.A.*
[62]*University of Michigan, Ann Arbor, Michigan 48109, U.S.A.*
[63]*Michigan State University, East Lansing, Michigan 48824, U.S.A.*
[64]*University of Mississippi, University, Mississippi 38677, U.S.A.*
[65]*University of Nebraska, Lincoln, Nebraska 68588, U.S.A.*
[66]*Princeton University, Princeton, New Jersey 08544, U.S.A.*
[67]*Columbia University, New York, New York 10027, U.S.A.*
[68]*University of Rochester, Rochester, New York 14627, U.S.A.*
[69]*State University of New York, Stony Brook, New York 11794, U.S.A.*
[70]*Brookhaven National Laboratory, Upton, New York 11973, U.S.A.*
[71]*Langston University, Langston, Oklahoma 73050, U.S.A.*
[72]*University of Oklahoma, Norman, Oklahoma 73019, U.S.A.*
[73]*Brown University, Providence, Rhode Island 02912, U.S.A.*
[74]*University of Texas, Arlington, Texas 76019, U.S.A.*
[75]*Southern Methodist University, Dallas, Texas 75275, U.S.A.*
[76]*Rice University, Houston, Texas 77005, U.S.A.*
[77]*University of Virginia, Charlottesville, Virginia 22901, U.S.A.*
[78]*University of Washington, Seattle, Washington 98195, U.S.A.*

(Received 20 May 2005; published 29 July 2005)

We present a measurement of the fraction f_+ of right-handed W bosons produced in top quark decays, based on a candidate sample of $t\bar{t}$ events in the lepton+jets decay mode. These data correspond to an integrated luminosity of 230 pb^{-1}, collected by the D0 detector at the Fermilab Tevatron $p\bar{p}$ Collider at $\sqrt{s} = 1.96$ TeV. We use a constrained fit to reconstruct the kinematics of the $t\bar{t}$ and decay products, which allows for the measurement of the leptonic decay angle θ^* for each event. By comparing the $\cos\theta^*$ distribution from the data with those for the expected background and signal for various values of f_+, we find $f_+ = 0.00 \pm 0.13(\text{stat}) \pm 0.07(\text{syst})$. This measurement is consistent with the standard model prediction of $f_+ = 3.6 \times 10^{-4}$.

DOI: 10.1103/PhysRevD.72.011104 PACS numbers: 14.65.Ha, 14.70.Fm, 12.15.Ji, 12.38.Qk

*Visitor from University of Zurich, Zurich, Switzerland.

The top quark is by far the heaviest of the known fermions and is the only one that has a Yukawa coupling of order unity to the Higgs boson in the standard model. The top quark is also unique in that it decays through the electroweak interaction before it can hadronize. In the standard model, the top quark decays via the $V-A$ charged current interaction, and almost always to a W boson and b quark. We search for evidence of new physics in the $t \rightarrow Wb$ decay by measuring the helicity of the W boson. The W bosons produced from these decays are predominantly in either a longitudinal or a left-handed helicity state with fractions f_0 and f_-, respectively. For any linear combination of V and A currents at the tWb vertex [1],

$$f_0 \approx \frac{m_t^2}{2M_W^2 + m_t^2 + m_b^2} = 0.703 \pm 0.012, \qquad (1)$$

where m_t is the mass of the top quark for which we use 175 ± 5 GeV (consistent with the world average [2]), M_W is the mass of the W boson, and m_b is the mass of the bottom quark. In this analysis, we fix f_0 at 0.7 and measure the positive helicity fraction f_+. In the standard model, f_+ is suppressed by a factor of $(m_b/m_t)^2$ and is predicted at next-to-leading order to be 3.6×10^{-4} [3]. A measurement of f_+ that differs significantly from this value would be an unambiguous indication of new physics. For example, an f_+ value of 0.3 would indicate a purely $V+A$ charged current interaction. A possible theoretical model that includes a $V+A$ contribution at the tWb vertex is an $SU(2)_L \times SU(2)_R \times U_Y(1)$ extension of the standard model [4]. Direct measurements of the longitudinal fraction found $f_0 = 0.91 \pm 0.39$ [5] and $f_0 = 0.56 \pm 0.31$ [6]. A recent direct measurement of f_+ set a limit of $f_+ < 0.18$ at the 95% C.L. [7]. In addition, measurements of the $b \rightarrow s\gamma$ decay rate have indirectly limited the $V+A$ contribution in top quark decays to less than a few percent [8]. However, direct measurements of the $V+A$ contribution are still necessary because the limit from $b \rightarrow s\gamma$ assumes that the electroweak penguin contribution is dominant.

The angular distribution ω of the W boson decay products with weak isospin $I_3 = -1/2$ (charged lepton or d, s quark) in the rest frame of the W boson can be described by introducing the angle $\theta^*$with respect to the top quark direction [1]:

$$\omega(\cos\theta^*) = \frac{3}{4}(1-\cos^2\theta^*)f_0 + \frac{3}{8}(1-\cos\theta^*)^2 f_- + \frac{3}{8}(1+\cos\theta^*)^2 f_+. \qquad (2)$$

Because of backgrounds and reconstruction effects, the distribution of $\cos\theta^*$ we observe differs from $\omega(\cos\theta^*)$. However, the shape of the measured $\cos\theta^*$ distribution depends on $f_+$and this dependence can be used to measure f_+. We do this by selecting a data sample enriched in $t\bar{t}$ events, reconstructing the four vectors of the two top quarks and their decay products using a kinematic fit, and then calculating $\cos\theta^*$. This distribution in $\cos\theta^*$ is compared with templates for different f_+ values using a binned maximum likelihood method.

The D0 detector [9] comprises three main systems: the central-tracking system, the calorimeters, and the muon system. The central-tracking system is located within a 2 T solenoidal magnet. The next layer of detection involves three liquid-argon/uranium calorimeters: a central section (CC) covering pseudorapidities [10] $|\eta| \lesssim 1$, and two end calorimeters (EC) extending coverage to $|\eta| \approx 4$, all housed in separate cryostats. The muon system is located beyond the calorimetry, and consists of a layer of tracking detectors and scintillation trigger counters before 1.8 T toroids, followed by two more similar layers after the toroids.

This measurement uses a data sample recorded by the D0 experiment corresponding to 230 ± 15 pb^{-1} of $p\bar{p}$ collisions at $\sqrt{s} = 1.96$ TeV. We consider $t\bar{t}$ candidate events selected in the lepton+jets channel where one of the W bosons from t or $\bar{t}$ decays into an electron or muon and a corresponding neutrino and the other W boson decays hadronically. The final state is therefore characterized by one charged lepton (e or μ), at least four jets (two of which are b jets), and significant missing transverse energy ($\not\!\!E_T$).

Two separate analyses are performed and the results are combined. One analysis uses kinematic information to select $t\bar{t}$ events (''kinematic analysis'') and the other uses b jet identification as well as kinematic information in order to improve the signal to background ratio (''b-tagged analysis''). A b jet is identified by a displaced secondary vertex close to an associated jet [11]. The kinematic analysis vetoes b-tagged events to simplify the combination of results with the b-tagged analysis. In both analyses, selected events arise predominantly from three sources: $t\bar{t}$ production, $W+$ jets production, and multijet production where one of the jets is misidentified as a lepton and spurious $\not\!\!E_T$ appears due to mismeasurement of the transverse energy in the event.

The event selection [12] requires an isolated lepton (e or μ) with transverse momentum $p_T > 20$ GeV, no other lepton with $p_T > 15$ GeV in the event, $\mathrm{E_T} > 20$ GeV, and at least four jets. Leptons are categorized in two classes, ''loose'' and ''tight,'' the latter being a subset of the first. Loose electrons are required to have $|\eta| < 1.1$ and are identified by their energy deposition and isolation in the calorimeter, their transverse and longitudinal shower shapes, and information from the tracking system. For tight identification, a discriminant combining the above information must be consistent with the expectations for a high-p_T isolated electron. Loose muons are identified using the information from the muon and the tracking systems. They are required to have $|\eta| < 2.0$ and to be isolated from jets. Tight muons must also pass stricter

isolation requirements based on the energy of calorimeter clusters and tracks around the muon. Only tight leptons are used in the final event selection. Jets are required to pass a rapidity [10] cut of $|y| < 2.5$ and, in the kinematic analysis, must have $p_T > 20$ GeV. The requirement that a b jet is present significantly reduces the background contamination in the b-tagged analysis and allows the use of a lower jet p_T cut of $p_T > 15$ GeV which increases the efficiency for signal events.

The top quark and the W boson four-momenta are reconstructed using a kinematic fit which is subject to the following constraints: two jets must form the invariant mass of the W boson, the lepton and the $\not\!\!E_T$ together with the neutrino p_z component must form the invariant mass of the W boson, and the masses of the two reconstructed top quarks must be equal to 175 GeV. The p_z component of the neutrino is reconstructed by exploiting the fact that the masses of the two top quarks are both set to be 175 GeV, and solving the resulting quadratic equation for p_z [13]. In the case where the two p_z solutions lead to different results of the kinematic fit, the one with the lower χ^2 (of the fit) is kept. Among the 12 possible jet combinations, the solution with the minimal χ^2 from the kinematic fit is chosen; Monte Carlo studies show this yields the correct solution in about 60% of all cases.

The $t\bar{t}$ signal events for seven different values of f_+, $f_+ = 0.00, \ldots, 0.30$ in steps of 0.05, are generated with the ALPGEN Monte Carlo (MC) program [14] for the parton-level process (leading order) and PYTHIA [15] for simulation of subsequent hadronization. The mass of the top quark is set to $m_t = 175$ GeV. As the interference term between $V - A$ and $V + A$ is suppressed by the small mass of the b quark and is therefore negligible [16], these samples can be used to create $\cos\theta^*$ templates for any f_+ value by a linear interpolation of the templates. All seven templates from these samples are normalized to unit area and a linear fit to the contents of each $\cos\theta^*$ bin as a function of f_+ is performed. This procedure effectively averages over statistical fluctuations in the generated MC samples, thus providing a more precise model of the $\cos\theta^*$ distribution. The MC samples used to model events with W bosons produced in association with jets ($W+$ jets) are also generated with ALPGEN, requiring the W boson to decay leptonically. The factorization scale Q is set to $Q^2 = M_W^2 + \sum m_T^2$ [14].

To determine the number of multijet background events, we compare samples selected with loose and tight leptons. Going from loose to tight samples decreases the number of events from N_ℓ to N_t. The relative selection efficiency between the loose and the tight lepton criteria is different for true leptons (ϵ_ℓ) and jets faking an isolated lepton (ϵ_j). We use these efficiencies, known from data control samples [12], to estimate the number of multijet background events: $N_{\rm m} = (\epsilon_\ell N_\ell - N_t)/(\epsilon_\ell - \epsilon_j)$. The kinematic analysis calculates $N_{\rm m}$ for each bin in the $\cos\theta^*$ distribution from the data sample to obtain the shape of the multijet $\cos\theta^*$ templates. For the b-tagged analysis, the multijet template is formed from data events after the event selection except that the leptons are required to satisfy the loose and to fail the tight criteria.

To discriminate between $t\bar{t}$ pair production and background, a discriminant $\mathcal{D}$ is built [12] using input variables which exploit the differences in event topology: H_T (defined as the scalar sum of the jet p_T values), the minimum dijet mass of the jet pairs, the χ^2 from the kinematic fit, the centrality (defined as H_T/H_E where H_E is the sum of the jet energies) [17], $K'_{\rm Tmin}$ (defined as the distance in $\eta - \phi$ space, where ϕ is the azimuthal angle, between the closest pair of jets multiplied by the p_T of the lowest-p_T jet in the pair and divided by the transverse energy of the reconstructed W boson) [13], and aplanarity and sphericity (calculated from the four leading jets and the lepton). The last two variables characterize the event shape and are defined, for example, in Ref. [18]. Only the four leading jets in p_T are considered in computing these variables to reduce the dependence on systematic effects from the modeling of soft radiation and underlying event processes. All of these variables are used for the discriminant in the kinematic analysis. Only H_T, centrality, the minimum dijet mass, and χ^2 are used in the b-tagged analysis. The discriminant is built separately for the kinematic and b-tagged analyses, using the method described in Refs. [12,13]. The distributions of signal (S) and background (B) events in each of the above variables are normalized to unity. For each variable v_i we fit a polynomial to the logarithm of S/B as a function of v_i. The discriminant is defined as

$$\mathcal{D}(v_1, v_2, \ldots) = \frac{\exp(\sum_i [\ln(S(v_i)/B(v_i))]_{\rm fit})}{\exp(\sum_i [\ln(S(v_i)/B(v_i))]_{\rm fit}) + 1}. \quad (3)$$

We select events for which $\mathcal{D} > 0.6$ in the kinematic analysis, and $\mathcal{D} > 0.25$ in the b-tagged analysis. These values are chosen to minimize the expected statistical uncertainty in the measurement of f_+ as determined by simulations of the analysis.

We then perform a binned maximum likelihood fit to compare the observed $\mathcal{D}$ distribution in the data to the sum

TABLE I. Number of events observed for each component (signal and backgrounds) of the kinematic and b-tagged samples, and the number of data events, after the cut on the discriminant $\mathcal{D}$ discussed in the text. The fits are made before the final cut on $\mathcal{D}$, so the sum of the components need not agree exactly with the observed numbers of events.

Event Class	Kinematic	b-tagged
$t\bar{t}$	16.5 ± 5.8	40.8 ± 8.1
$W+$ jets	14.3 ± 3.0	11.5 ± 4.1
Multijet	5.0 ± 2.1	1.5 ± 0.5
Data	35	52

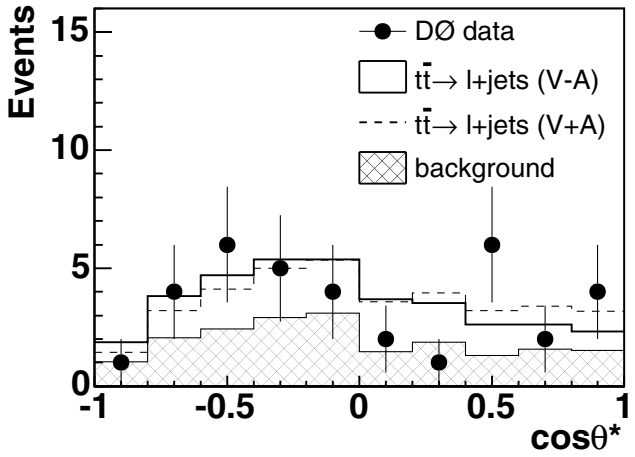

FIG. 1. $\cos\theta^*$ distribution observed in the kinematic analysis. The standard model prediction is shown as the solid line, while a model with a pure $V + A$ interaction would result in the distribution given by the dashed line.

of the distributions expected from $t\bar{t}$, $W+$ jets, and multijet events. The number of multijet events is constrained to a Poisson distribution with mean N_{m}. The likelihood is then maximized with respect to the number of $t\bar{t}$, $W+$ jets, and multijet events. We multiply these numbers by the efficiency for each type of event to pass the $\mathcal{D}$ selection to determine the composition of the sample used for measuring $\cos\theta^*$. Table I lists the composition of each sample as well as the number of observed events in the data. The $\cos\theta^*$ distribution obtained in data after the full selection is shown in Fig. 1 for the kinematic and in Fig. 2 for the b-tagged analysis.

A binned maximum likelihood fit of signal and background $\cos\theta^*$ templates to the data was used to measure

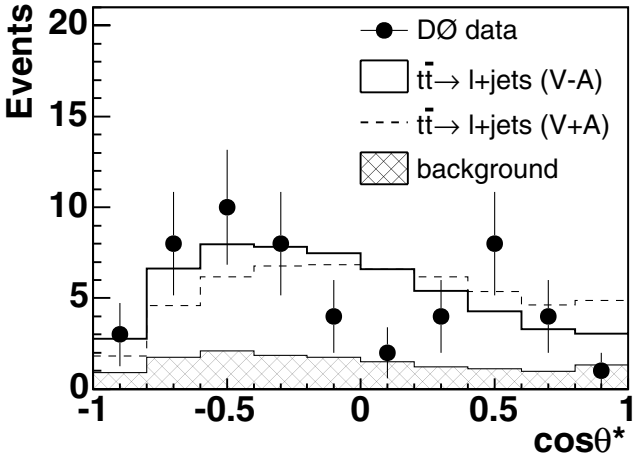

FIG. 2. $\cos\theta^*$ distribution observed in the b-tagged analysis. The standard model prediction is shown as the solid line, while a model with a pure $V + A$ interaction would result in the distribution given by the dashed line.

f_+. We compute the binned Poisson likelihood ($L(f_+)$) of the data to be consistent with the sum of signal and background templates, normalized to the numbers given in Table I, at each of the seven chosen f_+ values. In both analyses, a parabola is fit to the $-\ln[L(f_+)]$ points to determine the likelihood as a function of f_+.

Systematic uncertainties are evaluated in ensemble tests by varying the parameters (see Table II) which can affect the shape of the $\cos\theta^*$ distributions or the relative contribution from the three sources ($t\bar{t}$, $W+$ jets and QCD). Ensembles are formed by drawing events from a model with the parameter under study varied. These are compared to the standard $\cos\theta^*$ templates in a maximum likelihood fit. The average shift in the resulting f_+ value is taken as the systematic uncertainty and is shown in Table II. The total systematic uncertainty is then taken into account in the likelihood by convoluting the latter with a Gaussian with a width that corresponds to the total systematic uncertainty.

The top quark mass and the jet energy calibration (JEC) are the leading sources of systematic uncertainty. The mass of the top quark has been varied by ± 5 GeV with respect to $m_t = 175$ GeV and the JEC by $\pm 1\sigma$ around the nominal value. The statistical uncertainty on the $\cos\theta^*$ templates has been taken as a systematic uncertainty. It is estimated by fluctuating them according to their statistical uncertainty. Uncertainties in the modeling of the b-tag algorithm lead to uncertainties in the flavor composition of the $W+$ jets background and in the $\cos\theta^*$ distribution itself due to the p_T and η dependence of the b-tag algorithm [11]. An uncertainty in the flavor composition translates into a different shape of the $\cos\theta^*$ distribution and a difference in the signal to background ratio. In order to estimate the systematic uncertainty due to gluon radiation in $t\bar{t}$ events, an alternative signal sample of $t\bar{t}+$ jet has been generated with ALPGEN, and mixed with the default $t\bar{t}$ sample using the leading order cross sections for both processes. Effects of the choice of factorization scale Q in the generation of the $W+$ jets events have been evaluated by using a sample where $Q^2 = \langle p_T \rangle^2$ [14]. There is a systematic uncertainty due to the final sample composition obtained by the fit to the discriminant $\mathcal{D}$. The kinematic

TABLE II. Systematic uncertainties on f_+ for the two independent analyses and for the combination.

Source	Kinematic	b-tagged	Combined
Jet energy calibration	0.03	0.04	0.04
Top quark mass	0.04	0.04	0.04
Template statistics	0.05	0.02	0.03
b-tag	0.03	0.02	0.02
$t\bar{t}$model	0.01	0.02	0.02
$W+$ jets model	0.01	0.01	0.01
Sample composition	—	0.02	0.01
Calibration	0.01	0.01	0.01
Total	0.08	0.07	0.07

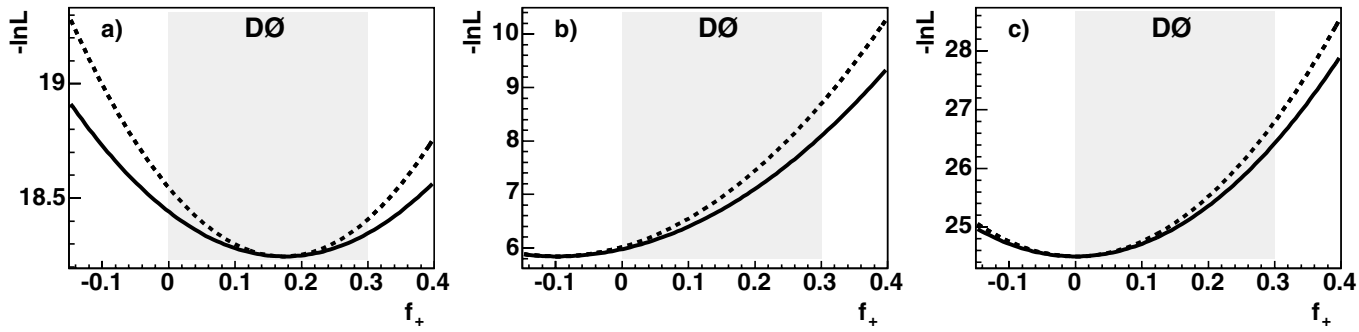

FIG. 3. $-\ln L$ curve obtained in the (a) kinematic analysis, (b) b-tagged analysis, and (c) kinematic and b-tagged analyses combined. The dashed line includes only the statistical uncertainty while the solid line also includes the systematic uncertainties. The physically allowed region for f_+ is indicated by the gray area.

analysis treats this uncertainty as a statistical uncertainty and includes it in the definition of the likelihood as described in Ref. [19] while in the b-tagged analysis this uncertainty is studied by changing the compositions within their errors. The difference found between the input f_+ value and the reconstructed f_+ value in ensemble tests is taken as systematic uncertainty on the calibration of the analysis.

The result of the maximum likelihood fit to the $\cos\theta^*$ distribution observed in the data is shown in Figs. 3(a) and 3(b) for the kinematic and b-tagged samples, respectively. The statistical uncertainties from the two individual analyses are 0.22 for the kinematic and 0.17 for the b-tagged analysis. The $-\ln[L(f_+)]$ curves for the kinematic and b-tagged measurements are combined, as shown in Fig. 3(c). The systematic uncertainties are assumed to be fully correlated except for the systematics on calibration of the individual analyses which are uncorrelated, and the Monte Carlo model systematics which are partially correlated. Assuming a fixed value of 0.7 for f_0, the combined result for f_+ is

$$f_+ = 0.00 \pm 0.13(\text{stat}) \pm 0.07(\text{syst}). \quad (4)$$

The observed combined statistical uncertainty (0.13) is in good agreement with the expectation (0.12) inferred from ensemble tests. We also calculate a Bayesian confidence interval (using a flat prior distribution which is nonzero only in the physically allowed region of $f_+ = 0.0 - 0.3$) which yields

$$f_+ < 0.25 \text{ at } 95\% \text{ C.L.} \quad (5)$$

The W boson positive helicity fraction f_+ that we have measured in $t\bar{t}$ decays in the lepton+jets channel is consistent with the standard model prediction of $f_+ = 3.6 \times 10^{-4}$ [3].

We thank the staffs at Fermilab and collaborating institutions, and acknowledge support from the DOE and NSF (U.S.A.); CEA and CNRS/IN2P3 (France); FASI, Rosatom and RFBR (Russia); CAPES, CNPq, FAPERJ, FAPESP, and FUNDUNESP (Brazil); DAE and DST (India); Colciencias (Colombia); CONACyT (Mexico); KRF (Korea); CONICET and UBACyT (Argentina); FOM (The Netherlands); PPARC (United Kingdom); MSMT (Czech Republic); CRC Program, CFI, NSERC, and WestGrid Project (Canada); BMBF and DFG (Germany); SFI (Ireland); Research Corporation, Alexander von Humboldt Foundation, and the Marie Curie Fellowships.

[1] G. L. Kane, G. A. Ladinsky, and C.-P. Yuan, Phys. Rev. D **45**, 124 (1992); R. H. Dalitz and G. R. Goldstein,*ibid.* **45**, 1531 (1992); C. A. Nelson *et al.*, Phys. Rev. D **56**, 5928 (1997).

[2] Review of particle physics, S. Eidelman *et al.*, Phys. Lett. B **592**, 1 (2004).

[3] M. Fischer *et al.*, Phys. Rev. D **63**, 031501(R) (2001).

[4] M. Beg *et al.*, Phys. Rev. Lett. **38**, 1252 (1977); S. H. Nam, Phys. Rev. D **66**, 055008 (2002).

[5] T. Affolder *et al.* (CDF Collaboration), Phys. Rev. Lett. **84**, 216 (2000).

[6] V. M. Abazov *et al.* (D0 Collaboration), Phys. Lett. B **617**, 1 (2005).

[7] D. Acosta *et al.* (CDF Collaboration), Phys. Rev. D **71**, 031101 (2005).

[8] K. Fujikawa and A. Yamada, Phys. Rev. D **49**, 5890 (1994); P. Cho and M. Misiak, Phys. Rev. D **49**, 5894 (1994); C. Jessop, SLAC Report No. SLAC-PUB-9610, 2002.

[9] V. M. Abazov *et al.* (D0 Collaboration),"The Upgraded D0 Detector," (to be published).
[10] Rapidity y and pseudorapidity η are defined as functions of the polar angle θ with respect to the proton beam and the parameter β as $y(\theta, \beta) \equiv \frac{1}{2} \ln[(1 + \beta\cos\theta)/(1 - \beta\cos\theta)]$ and $\eta(\theta) \equiv y(\theta, 1)$, where β is the ratio of a particle's momentum to its energy.
[11] V. M. Abazov *et al.* (D0 Collaboration), hep-ex/0504058.
[12] V. M. Abazov *et al.* (D0 Collaboration), hep-ex/0504043.
[13] B. Abbott *et al.* (D0 Collaboration), Phys. Rev. D **58**, 052001 (1998).
[14] M. L. Mangano *et al.*, J. High Energy Phys. 07 (2003) 001.
[15] T. Sjöstrand *et al.*, Comput. Phys. Commun. **135**, 238 (2001).
[16] J. G. Körner, (private communication).
[17] B. Abbott *et al.* (D0 Collaboration), Phys. Rev. D **60**, 012001 (1999).
[18] V. Barger *et al.*, Phys. Rev. D **48**, R3953 (1993).
[19] P. Bhat *et al.*, Phys. Lett. B **407**, 73 (1997).